Cellular/Molecular

$Na_v1.7$ Mutant A863P in Erythromelalgia: Effects of Altered Activation and Steady-State Inactivation on Excitability of Nociceptive Dorsal Root Ganglion Neurons

T. Patrick Harty,[1,2,3] Sulayman D. Dib-Hajj,[1,2,3] Lynda Tyrrell,[1,2,3] Rachael Blackman,[1,2,3] Fuki M. Hisama,[1] John B. Rose,[4] and Stephen G. Waxman[1,2,3]

[1]Department of Neurology and [2]Center for Neuroscience and Regeneration Research, Yale University School of Medicine, New Haven, Connecticut 06510, [3]Rehabilitation Research Center, Veterans Affairs Connecticut Healthcare System, West Haven, Connecticut 06516, and [4]Department of Anesthesiology and Critical Care Medicine, Children's Hospital of Philadelphia, Philadelphia, Pennsylvania 19104

Inherited erythromelalgia/erythermalgia (IEM) is a neuropathy characterized by pain and redness of the extremities that is triggered by warmth. IEM has been associated with missense mutations of the voltage-gated sodium channel $Na_v1.7$, which is preferentially expressed in most nociceptive dorsal root ganglia (DRGs) and sympathetic ganglion neurons. Several mutations occur in cytoplasmic linkers of $Na_v1.7$, with only two mutations in segment 4 (S4) and S6 of domain I. We report here a simplex case with an alanine 863 substitution by proline (A863P) in S5 of domain II of $Na_v1.7$. The functional effect of A863P was investigated by voltage-clamp analysis in human embryonic kidney 293 cells and by current-clamp analysis to determine the effects of A863P on firing properties of small DRG neurons. Activation of mutant channels was shifted by −8 mV, whereas steady-state fast inactivation was shifted by +10 mV, compared with wild-type (WT) channels. There was a marked decrease in the rate of deactivation of mutant channels, and currents elicited by slow ramp depolarizations were 12 times larger than for WT. These results suggested that A863P could render DRG neurons hyperexcitable. We tested this hypothesis by studying properties of rat DRG neurons transfected with either A863P or WT channels. A863P depolarized resting potential of DRG neurons by +6 mV compared with WT channels, reduced the threshold for triggering single action potentials to 63% of that for WT channels, and increased firing frequency of neurons when stimulated with suprathreshold stimuli. Thus, A863P mutant channels produce hyperexcitability in DRG neurons, which contributes to the pathophysiology of IEM.

Key words: **ion channel; neuropathic pain; erythermalgia; sensory neuron; voltage clamp; current clamp**

Introduction

Primary erythromelalgia, also called erythermalgia, is a debilitating disorder characterized by redness and pain in the feet and hands that can be triggered by warmth or mild exercise (van Genderen et al., 1993). Symptoms begin in early childhood and are often unresponsive to pharmacotherapy. The condition is inherited in an autosomal dominant manner (Finley et al., 1992) and has recently been shown to be caused by missense mutations in *SCN9A*, the gene that encodes the voltage-gated sodium channel α-subunit $Na_v1.7$ (Yang et al., 2004; Dib-Hajj et al., 2005; Drenth et al., 2005; Michiels et al., 2005; Han et al., 2006).

$Na_v1.7$ is preferentially expressed in dorsal root ganglia (DRGs) and sympathetic ganglia (Black et al., 1996; Sangameswaran et al., 1997; Toledo-Aral et al., 1997), and its expression is increased in DRG neurons under inflammatory conditions (Black et al., 2004). DRG-specific knock-out of $Na_v1.7$ channels in mice leads to a substantial increase in thermal and mechanical pain thresholds (Nassar et al., 2004). $Na_v1.7$ channels are blocked by nanomolar concentrations of tetrodotoxin (TTX). They are characterized by fast activation and inactivation (Klugbauer et al., 1995; Sangameswaran et al., 1997) and slow recovery from inactivation. In addition, a slow rate of closed-state inactivation underlies an ability to generate a response, close to resting potential, to slow depolarizations (Cummins et al., 1998; Herzog et al., 2003). These findings support the idea that $Na_v1.7$ channels play an important role in pain sensation.

Initial biophysical studies with mutant $Na_v1.7$ (L858H and I848T) channels demonstrated a number of changes in voltage-dependent properties compared with wild-type (WT) $Na_v1.7$ channels, including hyperpolarizing shifts in activation, decreased rates of deactivation, and larger ramp responses (Cummins et al., 2004). These changes are predicted to increase DRG neuron excitability. Subsequent studies with the L858H mutation (Rush et al., 2006) demonstrated that small DRG neurons expressing the mutant channels are hyperexcitable, as evidenced by a decrease in action potential threshold and an increase in frequency of firing compared with cells transfected with the WT channel. Additional biophysical studies with a third mutation, F1449V (Dib-Hajj et al., 2005), demonstrated a depolarizing shift

Received June 13, 2006; revised Oct. 25, 2006; accepted Oct. 25, 2006.

This work was supported by the Medical Research Service and Rehabilitation Research Service, Department of Veterans Affairs and by grants from the National Multiple Sclerosis Society and the Erythromelalgia Association. F.M.H. was supported by a Paul Beeson Scholar Award (American Federation for Aging Research). The Center for Neuroscience and Regeneration Research is a collaboration of the Paralyzed Veterans of America and the United Spinal Association with Yale University.

Correspondence should be addressed to Dr. Stephen G. Waxman, Department of Neurology, LCI 707, Yale Medical School, P.O. Box 208018, New Haven, CT 06520. E-mail: Stephen.Waxman@yale.edu.

DOI:10.1523/JNEUROSCI.3424-06.2006

 0270-6474/06/2612566-10$15.00/0

in steady-state fast inactivation in addition to the hyperpolarizing shift in activation. Interestingly, this mutation did not exhibit the decrease in deactivation rate and increased ramp currents observed with L858H and I848T. However, action potential thresholds were decreased, and firing frequency increased, indicating an increase in excitability of small, nociceptive DRG neurons.

In this study, we profiled the *SCN9A* sequence from an adolescent male patient with early-onset inherited erythromelalgia/erythermalgia (IEM) and with a negative family history, and we identified a missense mutation involving substitution of alanine 863 in domain II (DII)/segment 5 (S5) with proline (A863P). We also investigated the functional effects of this substitution by studying biophysical properties of the mutant channels and their ability to affect the excitability of DRG neurons, and we propose a mechanism whereby the mutant channels produce hyperexcitability in nociceptive DRG neurons.

Materials and Methods

Exon screening. Studies were performed according to an ethically approved institutional protocol. Genomic DNA (gDNA) was purified from buccal swabs or venous blood. Human variation panel control DNA (25 white males, 25 white females) was obtained from the Coriell Institute (Camden, NJ). All coding exons and flanking intronic sequences, as well as exons encoding 5′ and 3′ untranslated sequences within the cDNA sequence, were amplified and sequenced as described previously (Dib-Hajj et al., 2005). Briefly, PCR amplification was performed using 150 ng of gDNA, 1 μM primers, and Expand Long Template polymerase (Roche Diagnostics, Indianapolis, IN) in a 50 μl reaction for 35 cycles (95°C for 30 s, 55°C for 30 s, and 72°C for 1 min). All exons and flanking intronic sequences were amplified using two primers, except exon 26, which required four sets of primers to cover its entirety. Genomic sequences were compared with the reference $Na_v1.7$ cDNA (Klugbauer et al., 1995) to identify sequence variation. Sequencing was performed at the Howard Hughes Medical Institute/Keck Biotechnology Center at Yale University (New Haven, CT). Sequence analysis used BLAST (basic local alignment search tool; National Library of Medicine, Bethesda, MD) and Lasergene (DNAStar, Madison, WI).

Voltage-clamp electrophysiology. The plasmid carrying the TTX-resistant (TTX-r) version of human $Na_v1.7$ cDNA ($hNa_v1.7_R$) was described previously (Herzog et al., 2003). The A863P mutation was introduced into $hNa_v1.7_R$ using QuikChange XL site-directed mutagenesis (Stratagene, La Jolla, CA). WT or A863P mutant $hNa_v1.7_R$ α subunits were cotransfected with the human β1 and β2 subunits (Lossin et al., 2002) into human embryonic kidney 293 (HEK293) cells using Lipofectamine reagent (Invitrogen, Carlsbad, CA). HEK293 cells were grown under standard culture conditions (5% CO_2, 37°C) in DMEM supplemented with 10% fetal bovine serum.

Whole-cell voltage-clamp recordings were performed on isolated, green fluorescent protein (GFP)-labeled HEK293 cells at room temperature (20–22°C) within 24–40 h of transfection. Electrodes were pulled from 1.6 mm outer diameter borosilicate glass micropipettes (World Precision Instruments, Sarasota, FL) and had a resistance of 1–1.5 MΩ when filled with pipette solution. The pipette solution contained the following (in mM): 140 CsF, 10 NaCl, 10 HEPES, and 1 EGTA, pH 7.3 with CsOH (adjusted to 320 mOsm with dextrose). The extracellular solution contained the following (in mM): 140 NaCl, 3 KCl, 1 $MgCl_2$, 1 $CaCl_2$, and 10 HEPES, pH 7.3 with NaOH (adjusted to 320 mOsm with dextrose). Solution was applied to the recording chamber via gravity perfusion and removed by vacuum suction. Voltage-clamped currents were recorded on an Axopatch 200B amplifier (Molecular Devices, Sunnyvale, CA) and stored on a personal computer via a Digidata 1322a analog-to-digital converter (Molecular Devices) at an acquisition rate of 50 kHz with a low-pass Bessel filter setting of 5 kHz. Voltage errors were minimized with 85% series resistance compensation, and when appropriate, linear leak currents and capacitance artifacts were subtracted out using the P/N method provided by Clampex (Molecular Devices) acquisition software. Data acquisition began 3 min after establishing whole-cell configuration. Clampfit (Molecular Devices) and Origin (Microcal Software, Northampton, MA) were used for data analysis. To generate activation curves, cells were held at −100 mV and stepped to potentials of −80 to 40 mV for 100 ms. Peak inward currents obtained from activation protocols were converted to conductance values using the equation $G = I/(V_m - E_{Na})$, where G is the conductance, I is the peak inward current, V_m is the membrane potential step used to elicit the response, and E_{Na} is the reversal potential for sodium (determined for each cell using the x-axis intercept of a linear fit of the peak inward current responses to the last four voltage steps of the activation protocol). Conductance data were normalized by the maximum conductance value and fit with a Boltzmann equation of the form $G/G_{max} = 1/(1 + \exp[(V_{1/2} - V_m)/k])$, where $V_{1/2}$ is the midpoint of activation, and k is a slope factor. To generate steady-state fast inactivation curves, cells were stepped to inactivating potentials of −130 to 10 mV for 500 ms, followed by a 20 ms step to 0 mV. The protocol for slow inactivation consisted of a 30 s step to potentials varying from −120 to 10 mV, followed by a 100 ms step to −120 mV to remove fast inactivation and a 20 ms step to 0 mV to elicit a test response. Peak inward currents obtained from steady-state fast inactivation and slow inactivation protocols were normalized by the maximum current amplitude and fit with a Boltzmann equation of the form $I/I_{max} = 1/(1 + \exp[(V_m - V_{1/2})/k])$, where V_m represents the inactivating prepulse membrane potential and $V_{1/2}$ represents the midpoint of inactivation. Decaying currents were fit with a single exponential equation of the form $I = A \times \exp(-t/\tau) + I_c$, where A is the amplitude of the fit, t is time, τ is the time constant of decay, and I_c is the asymptotic minimum to which the currents decay. Data are expressed as means ± SE. Statistical significance was determined by Student's t test.

Transfection of DRG neurons and current-clamp electrophysiology. We harvested DRG tissue from deeply anesthetized (ketamine/xylazine, 80/10 mg/kg, i.p.) 1- to 5-d-old Sprague Dawley rats, and we isolated neurons as described previously (Rizzo et al., 1994). Sodium channel and GFP constructs (channel:GFP ratio of 5:1) were electroporated into DRG neurons using Rat Neuron Nucleofector Solution (Amaxa, Gaithersburg, MD) with WT $Na_v1.7_R$ or the A863P mutant derivative as described previously (Dib-Hajj et al., 2005; Rush et al., 2006). Transfected DRG neurons were incubated at 37°C in Ca^{2+}- and Mg^{2+}-free culture medium (DMEM plus 10% fetal calf serum) for 5 min to increase cell viability. The cell suspension was then diluted in culture medium supplemented with NGF and GDNF (glial cell line-derived neurotrophic factor) (50 ng/ml), plated on 12 mm circular coverslips coated with laminin and poly-ornithine, and incubated at 37°C in 5% CO_2.

Small (20–25 μm) GFP-labeled DRG neurons were used for current-clamp recording 24–40 h after transfection. Electrodes had a resistance of 1–2 MΩ when filled with the pipette solution, which contained the following (in mM): 140 KCl, 0.5 EGTA, 5 HEPES, and 3 Mg-ATP, pH 7.3 with KOH (adjusted to 315 mOsm with dextrose). The extracellular solution contained the following (in mM): 140 NaCl, 3 KCl, 2 $MgCl_2$, 2 $CaCl_2$, 10 HEPES, pH 7.3 with NaOH (adjusted to 320 mOsm with dextrose). Solution application and signal acquisition were the same as for voltage-clamp recording. Whole-cell configuration was obtained in voltage-clamp mode before proceeding to the current-clamp recording mode. Cells with stable (<10% variation) resting membrane potentials (RMPs) more negative than −35 mV and overshooting action potentials (>85 mV RMP to peak) were used for additional data collection. Input resistance was determined by the slope of a line fit to hyperpolarizing responses to current steps of 10–35 pA. Threshold was determined by the first action potential elicited by a series of depolarizing current injections that increased in 5 pA increments.

Student's t test was used to assess the significance of differences between RMP, input resistance, and spike amplitude. ANOVA methods were used to analyze the frequency of firing data. The Mann–Whitney U test was used to assess the statistical significance of action potential threshold data, because the data did not meet the normal distribution criteria for Student's t test.

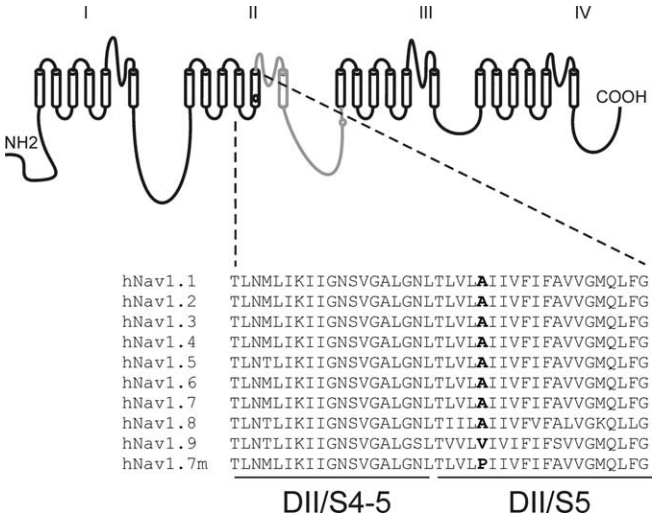

Figure 1. Schematic of a voltage-gated sodium channel α subunit showing the location of the A863P mutation and the aligned sequences for the Na_v1 DII/S4–S5 linker and DII/S5. A863 is conserved in eight of the nine known voltage-gated sodium channels. hNav1.7m, Mutated $hNa_v1.7$.

Results

Mutation in exon 15

A 14-year-old white male with excruciating pain, warmth, and redness of both feet has been followed in the Pain Management Clinic at the Children's Hospital of Philadelphia (Philadelphia, PA) for >2 years. Symptoms started in preschool and currently occur up to 20 times per day. Initially, the patient's symptoms were successfully treated with intravenous lidocaine and, subsequently, oral mexiletine. The number of pain episodes was reduced to <4 per day, as was the pain associated with these episodes. However, after 6 months, the treatment became gradually less effective, and the number of pain episodes has returned to previous levels. The redness and warmth have spread proximally over the last 2 years to include not only his feet but also his lower legs to a point midway between the ankles and knees, and he has begun to experience milder pain, redness, and warmth in the palms of his hands as well. Based on the clinical evaluation, the patient was diagnosed with possible primary erythromelalgia (Nathan et al., 2005). However, there is no family history of primary erythromelalgia or any other chronic pain condition.

Genomic DNA from the proband and his family (mother, father, and a sibling) was used to amplify all known exons of *SCN9A*, and their sequences were compared with $Na_v1.7$ cDNA (Klugbauer et al., 1995). Proband and control templates produced similar amplicons, which were purified and sequenced. Sequence analysis identified a G-to-C transversion in exon 15 (E15), corresponding to position 2587 of the reference sequence (Klugbauer et al., 1995). This mutation substitutes alanine by proline at position 863 of the polypeptide, located at the N terminus of transmembrane segment 5 in domain II. A863 is conserved in all human sodium channels except $Na_v1.9$, in which it is replaced by valine (Fig. 1).

The G2587C mutation destroys one of two restriction sites for *Msc*I (TGGCCA) in the exon 15 amplicon (624 bp), which facilitated screening of control samples. The amplicon from the asymptomatic parents and sibling produced the expected wild-type restriction digest pattern, whereas the proband showed an additional band consistent with the loss of the second *Msc*I site (data not shown). Restriction analysis of the amplicons from 50 ethnically matched control samples (100 chromosomes) showed only the expected wild-type pattern. Segregation of the G2587C mutation with IEM was confirmed by DNA sequencing of E15 from the proband, his family members, and five control samples.

Sequence analysis identified a second substitution (C3448T) in E18 of the proband *SCN9A* genomic DNA, which causes a substitution of arginine 1150 with tryptophan (R1150W). Also, the C3448T substitution destroys the unique *Rsa*I restriction enzyme site (GTAC) in this amplicon (381 bp). The R1150W substitution has been reported in a sporadic case of EM but was considered to be a benign polymorphism, because the codon usage is not conserved in the $Na_v1.7$ channels in different mammalian species (Drenth et al., 2005). We screened the family members and the ethnically matched control samples using restriction enzyme analysis to determine whether R1150W segregates with the disease phenotype. Restriction enzyme analysis of E18 amplicons determined that the asymptomatic father is homozygous for the C3448T substitution, the mother is homozygous for the wild-type allele, and the asymptomatic brother is heterozygous for the C3448T allele (data not shown). Additionally, restriction enzyme analysis of the 100 control chromosomes showed a loss of the *Rsa*I site in 14% of the alleles. Therefore, R1150W substitution reflects a low-frequency allele, which may not contribute to the disease phenotype.

Voltage-clamp electrophysiology

To investigate the effect of the A863P mutation on sodium channel activation, HEK293 cells transiently transfected with either the $Na_v1.7_R$ WT or A863P mutant construct were held at −100 mV and stepped to test potentials between −80 and 40 mV for 100 ms. Inward currents produced by this protocol are shown in Figure 2 for WT (*A*) and A863P (*B*) channels. Peak inward currents varied between 1 and 12 nA for all cells tested. The average peak inward current was larger for WT channels (4.3 ± 0.5 nA; $n = 33$) than for the A863P channels (2.2 ± 0.3 nA; $n = 21$). The larger peak currents for WT channels led to a significant difference in peak current density (WT, 260 ± 30 pA/pF; A863P, 90 ± 20 pA/pF; $t = 4.3$; $p < 0.001$).

As shown in Figure 2*C*, currents produced by the mutant channels both activated and reached maximum values at more hyperpolarized test potentials than the WT channels. Boltzmann fits of conductance (Fig. 2*E*) confirmed that the A863P mutation shifted activation in the hyperpolarizing direction. The midpoint of activation for mutant channels was −23.6 ± 0.6 mV ($k = 8.4 \pm 0.2$; $n = 21$) compared with −15.9 ± 0.8 mV ($k = 7.3 \pm 0.1$; $n = 33$) for WT channels. The difference in activation midpoints represented a significant hyperpolarizing shift of −7.7 mV ($t = 7.0$; $p < 0.001$). The A863P mutation also resulted in a shift in the voltage dependence of steady-state fast inactivation, without a significant effect on the kinetics of fast inactivation. As shown in Figure 2*D*, single exponential fits of sodium current decay demonstrated that fast inactivation occurred at the same rate for the WT and A863P mutant currents. However, Boltzmann fits of the voltage dependence of fast inactivation (Fig. 2*E*) revealed a depolarizing shift in the midpoint of inactivation for the A863P mutant ($V_{1/2} = -67.1 \pm 0.9$ mV; $k = 6.4 \pm 0.2$) relative to the WT ($V_{1/2} = -76.9 \pm 0.8$ mV; $k = 6.9 \pm 0.1$). The difference between the two inactivation midpoints represented a significant depolarizing shift of 9.8 mV ($t = 7.4$; $p < 0.001$). As shown in Figure 2*F*, the combination of a hyperpolarizing shift in activation and a depolarizing shift in fast inactivation led to a marked increase in the overlap of these two processes. This overlap predicts a window current, the fraction of peak sodium current that would be active at a given resting membrane potential.

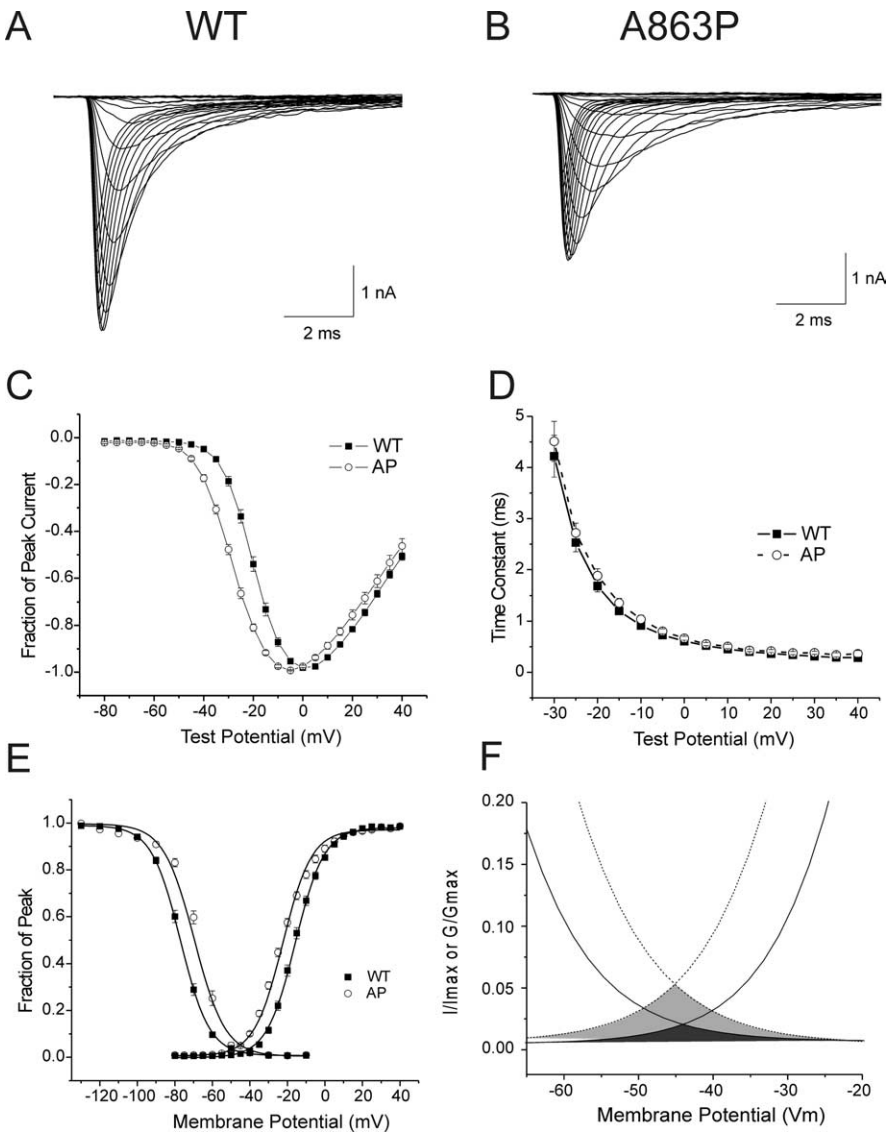

Figure 2. A863P shifts the voltage dependence of activation and steady-state fast inactivation without changing the kinetics of inactivation. ***A***, ***B***, Inward currents recorded from voltage-clamped HEK293 cells expressing WT (***A***) and A863P mutant (***B***) $Na_v1.7$ sodium channels. Cells were held at −100 mV and stepped to membrane potentials from −80 to 40 mV for 100 ms in 5 mV steps. ***C***, Normalized peak current–membrane voltage relationship for activation of WT (■; $n = 33$) and A863P (AP; ○; $n = 21$) channels. ***D***, Voltage dependence of fast inactivation time constants for WT (■) and A863P (○) channels. Time constants were obtained from single exponential fits of current decay after peak responses to activation voltage steps such as those shown in ***A*** and ***B***. ***E***, Comparison of the voltage dependence of activation and steady-state fast inactivation for WT (■) and A863P (○) channels. Activation data were obtained by converting peak inward current to conductance, normalizing those data (see Materials and Methods), and fitting with a Boltzmann equation (lines on the right). Steady-state fast inactivation data were obtained by stepping cells to a prepulse membrane potential (varied from −130 to −10 mV) for 500 ms, followed by a 20 ms test pulse to 0 mV. The peak current in response to the test pulse was normalized by the maximum response amplitude, plotted as a function of prepulse membrane potential, and fit with a Boltzmann equation (lines on the left). ***F***, Expanded view of the area of overlap (shading) of activation and inactivation Boltzmann fits from ***E***. WT data are shown by solid lines and dark shading; A863P data are shown by dotted lines and light shading. Error bars represent SE.

To estimate the potential effect of an increased window current on RMP, we first used the overlapping activation/inactivation Boltzmann curves (Fig. 2*F*) to determine the fraction of sodium channels activated at the peak of the window current. At this membrane potential (−45 mV), 5% of the A863P channels are in a non-inactivated (available for activation) state, and 5% of the available channels are activated. The number of channels open at −45 mV is the product of these two fractions, or 0.25% of the total number of channels (peak sodium current). For WT channels, this value is 0.04% (2% × 2%). Small DRG neurons produce an average TTX-sensitive (TTX-s) sodium current of 15.4 nA (Rush et al., 2005). If $Na_v1.7$ channels produced 100% of the TTX-s current, the maximum peak window current would be 0.039 nA for A863P (0.25% of peak current) and 0.006 nA (0.04%) for WT channels. For an input resistance of 500 MΩ (this study; Renganathan et al., 2001), a 0.039 nA current would produce a membrane depolarization of 19.5 mV (500 MΩ × 0.039 nA) in small DRG neurons with A863P channels and 3 mV in neurons with WT channels, resulting in a difference of 16.5 mV. However, although biophysical data (Cummins et al., 1998; Herzog et al., 2003) and mRNA levels (Black et al., 1996) indicate that $Na_v1.7$ contributes substantially to the TTX-s currents in small DRG neurons, other TTX-s sodium channels ($Na_v1.6$ and $Na_v1.1$) are present (Black et al., 1996). To accommodate uncertainty about the level of $Na_v1.7$ contribution to TTX-s currents, we recalculated the depolarization produced by window currents based on a 50% contribution of $Na_v1.7$ to total TTX-s current, yielding an estimated membrane depolarization of 8.1 mV. Thus, in a cell lacking other voltage-gated ion channels, the increased window current observed for the A863P mutant channels would be expected to depolarize RMP by 8.1–16.5 mV. In DRG cells, this change is likely to be tempered but not eliminated by the presence of other voltage-gated ion channels, such as potassium channels, which activate in this voltage range.

The A863P mutant produced a significantly slower deactivation of sodium currents. After activation with a short (0.5 ms) depolarizing voltage step (Fig. 3*A*), WT sodium channels deactivated with a relatively fast time course that increased as a function of the membrane potential after the depolarizing step. As shown in Figure 3*B*, the A863P mutation produced a significant decrease in the rate of current decay across all deactivation potentials tested. The difference in decay rates was most notable at the most depolarized membrane potential tested (40 mV), at which WT currents decayed with a time constant of 0.13 ± 0.01 ms ($n = 10$), and A863P currents decayed with a time constant of 0.75 ± 0.08 ms ($n = 10$; $t = 8.03$; $p < 0.01$). Slowing of $Na_v1.7$ deactivation has been predicted to contribute to DRG excitability by prolonging responses after the cessation of a depolarizing stimulus (Cummins et al., 2004).

The effect of the A863P mutation on closed-state inactivation was tested by stepping from a membrane potential of −100 mV to more depolarized potentials that were below the threshold for current activation (−90 to −50 mV), followed by a depolarizing

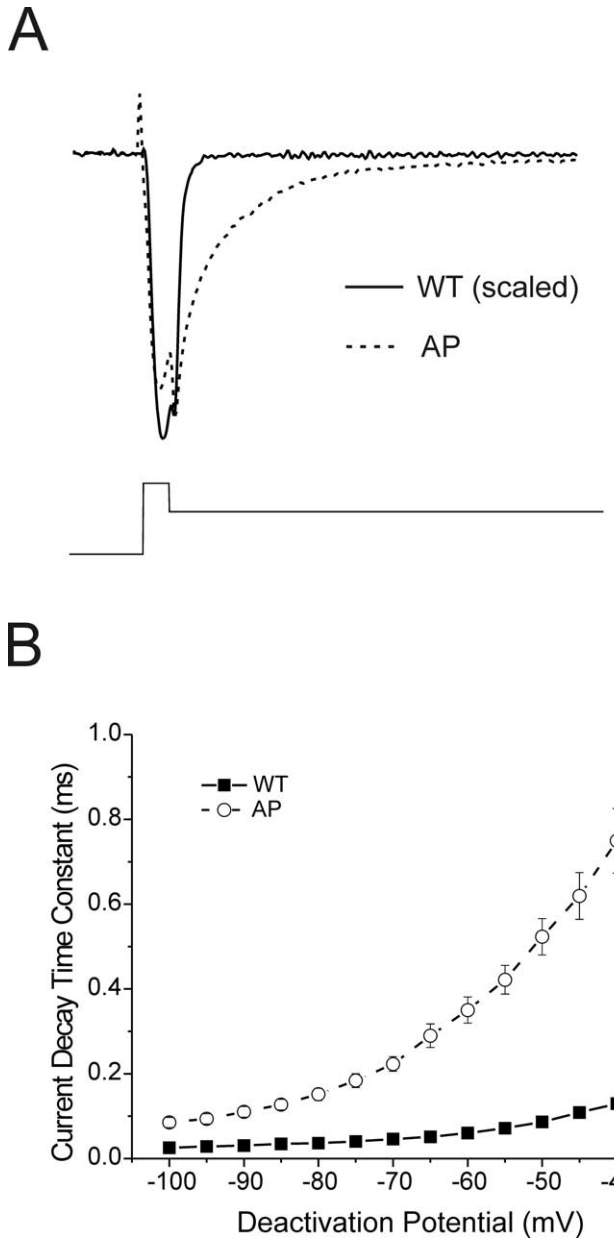

Figure 3. Deactivation is slowed by the A863P mutation. ***A***, Top, Currents recorded from two different HEK293 cells expressing WT (solid line) or A863P (AP; dotted line) sodium channels. Currents were elicited by a deactivation protocol (bottom) involving a short (0.5 ms) depolarizing step to 0 mV from a holding potential of −100 mV, followed by a hyperpolarizing step, which varied from −100 to −40 mV (step to −40 mV shown). To compare the kinetics of current decay, the WT current peak was scaled to match the A863P current peak. ***B***, Voltage dependence of deactivation current decay. Current decay after the depolarizing pulse was fit with a single exponential and plotted as a function of the hyperpolarizing step for WT (■; $n = 10$) and A863P (○; $n = 10$) data. Error bars represent SE.

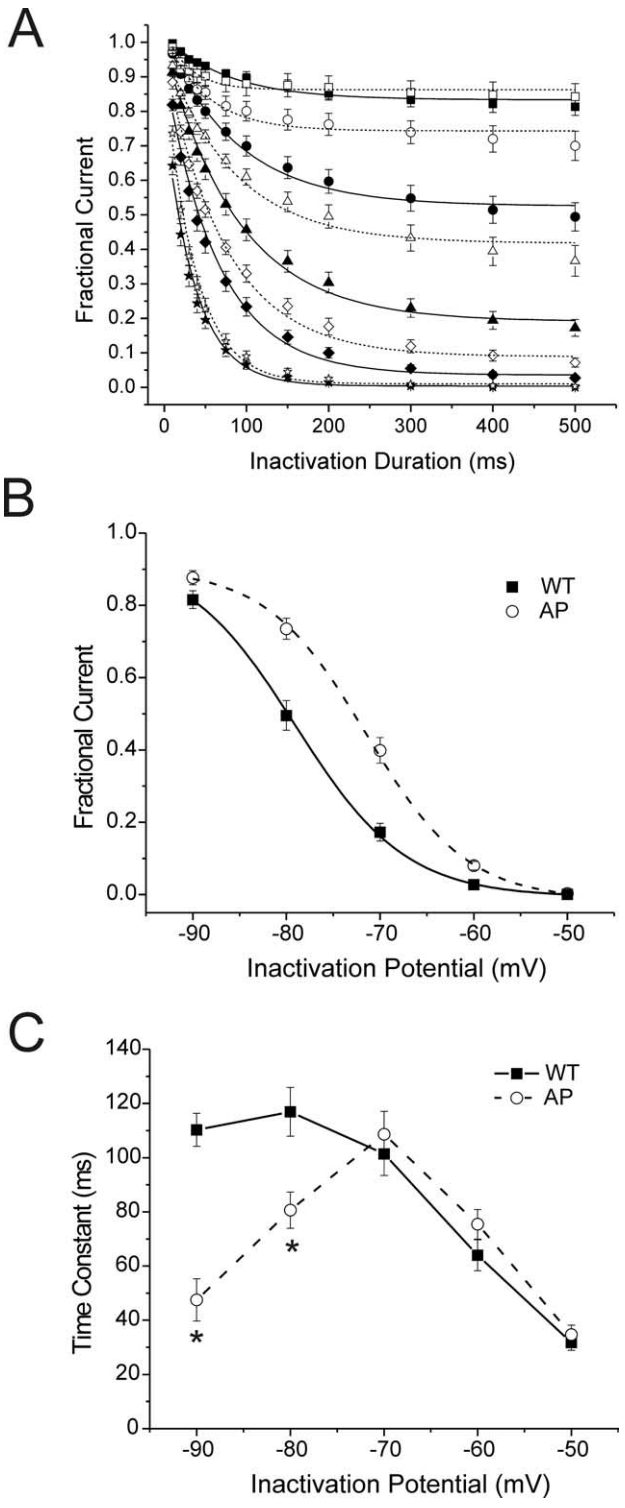

Figure 4. Changes in closed-state inactivation associated with the A863P mutation. ***A***, Summary of data used to determine voltage-dependent properties of closed-state inactivation in ***B*** and ***C*** below. Closed-state inactivation protocols used inactivating prepulses with durations that varied from 10 to 500 ms and five inactivation potentials (stars, −50 mV; diamonds, −60 mV; triangles, −70 mV; circles, −80 mV; and squares, −90 mV). Data were fit with single exponentials, and the resulting time constants were plotted as a function of prepulse membrane potential. Closed and open symbols represent data from cells expressing WT and A863P (AP) channels, respectively. ***B***, Voltage dependence of steady-state closed-state inactivation for WT (filled squares; $n = 19$) and A863P (open circles; $n = 10$) channels using a prepulse duration of 500 ms. Curves represent Boltzmann fits for WT (solid) and AP (dashed) data. See Results for details of voltage protocol. ***C***, Voltage dependence of the development of closed-state inactivation. Time constants resulting from single exponential fits in ***A*** are plotted as a function of inactivation potential. *$p < 0.05$. Error bars represent SE.

step to 0 mV to activate available channels. As shown in Figure 4*B*, for steady-state conditions (a prepulse duration of 500 ms), the A863P mutation shifted the voltage dependence of closed-state inactivation in the depolarizing direction by 7.6 mV (WT, −79.1 mV, $k = 5.9$; A863P, −71.5 mV, $k = 5.4$). This is similar to the 9.8 mV depolarizing shift in the voltage dependence of steady-state fast inactivation. We also looked at the development of closed-state inactivation by varying the duration of the depolarizing prepulse. Normalized current amplitudes were plotted as a function of prepulse duration and fit with single exponentials

(Fig. 4*A*). The resulting time constants were expressed as a function of the inactivating prepulse potential (Fig. 4*C*). The development of closed-state inactivation was faster for the A863P mutant channels, but only for the more hyperpolarized prepulse potentials (−80 and −90 mV).

Additional experiments were performed to further characterize the effects of the A863P mutation on the inactivation properties of $Na_v1.7$ sodium channels. First, we investigated the recovery of sodium channels from fast inactivation using a two-pulse protocol and varying the interpulse interval as well as the membrane potential maintained during the recovery interval. The amplitude of the second pulse was plotted as a function of interpulse interval and fit with single exponentials. Plotting the resulting time constants with respect to the recovery membrane potential (Fig. 5*A*) revealed that sodium channels containing the A863P mutation recovered more quickly than WT channels for recovery potentials between −100 and −80 mV, with the biggest difference at −80 mV (τ for WT = 77 ± 6 ms; τ for A863P = 42 ± 6 ms; $t = 3.7$; $p < 0.002$). $Na_v1.7$ channels inactivate with at least two different time courses. In addition to the fast time course (occurring within 10–100 ms), slow inactivation also occurs over a longer time course (1–10 s). To determine the effects of the A863P mutation on slow inactivation, cells were held at a potential between −120 and 10 mV for 30 s to allow for full development of both fast and slow inactivation. A 100 ms pulse to −120 mV was used to recover from fast inactivation, followed by a depolarizing pulse to activate the available channels. WT $Na_v1.7$ channels were slowly inactivated over a range of membrane potentials from −120 to −20 mV. Fit with a Boltzmann equation (Fig. 5*B*), the midpoint of inactivation was −80.0 ± 1.4 mV ($n = 16$), with a slope factor $k = 15.8 \pm 0.6$. Channels containing the A863P mutation had a midpoint of inactivation of −79.5 ± 2.1 mV ($n = 10$), which did not differ significantly from that of WT channels ($t = 0.2$; $p > 0.05$). However, mutant channels slowly inactivated over a much narrower voltage range (−110 to −50 mV; slope factor $k = 5.4 \pm 0.3$). The difference in slope factors between the two channel types was highly significant ($t = 13.4$; $p < 0.001$).

As a final test of the effects of the A863P mutation on voltage-gated sodium currents mediated by $Na_v1.7$ channels, we examined inward currents produced by slow ramp depolarizations. $Na_v1.7$ channels are thought to contribute to DRG excitability in part by generating slow depolarizations that boost subthreshold stimuli (Cummins et al., 1998). In support of this hypothesis, DRG neurons and cells that have been transfected with $Na_v1.7$ respond to a slow depolarizing ramp voltage (−100 to 20 mV over 600 ms) with a small inward current. For WT channels, these currents are typically 0.1–1% of the maximum sodium current (Fig. 6). For cells transfected with the A863P mutation, the average current elicited by ramp depolarization (3.6 ± 0.6%; $n = 19$) was 12 times the size of the average current produced by WT channels (0.3 ± 0.1%; $n = 27$; $t = 6.2$; $p < 0.001$). In addition, the onset of the currents occurred at more hyperpolarized potentials for cells expressing the mutation (−56.8 ± 1.5 mV) than for the WT cells (−51.3 ± 2.2 mV; $t = 2.69$; $p = 0.01$). The peak current also occurred at more hyperpolarized potentials (A863P, −37.3 ± 1.0 mV; WT, −28.3 ± 2.7 mV; $t = 3.57$; $p < 0.01$). To the extent that ramp-evoked currents are an indication of the contribution of $Na_v1.7$ channels to cell excitability, these results suggest that the A863P mutation should produce hyperexcitability in DRG neurons.

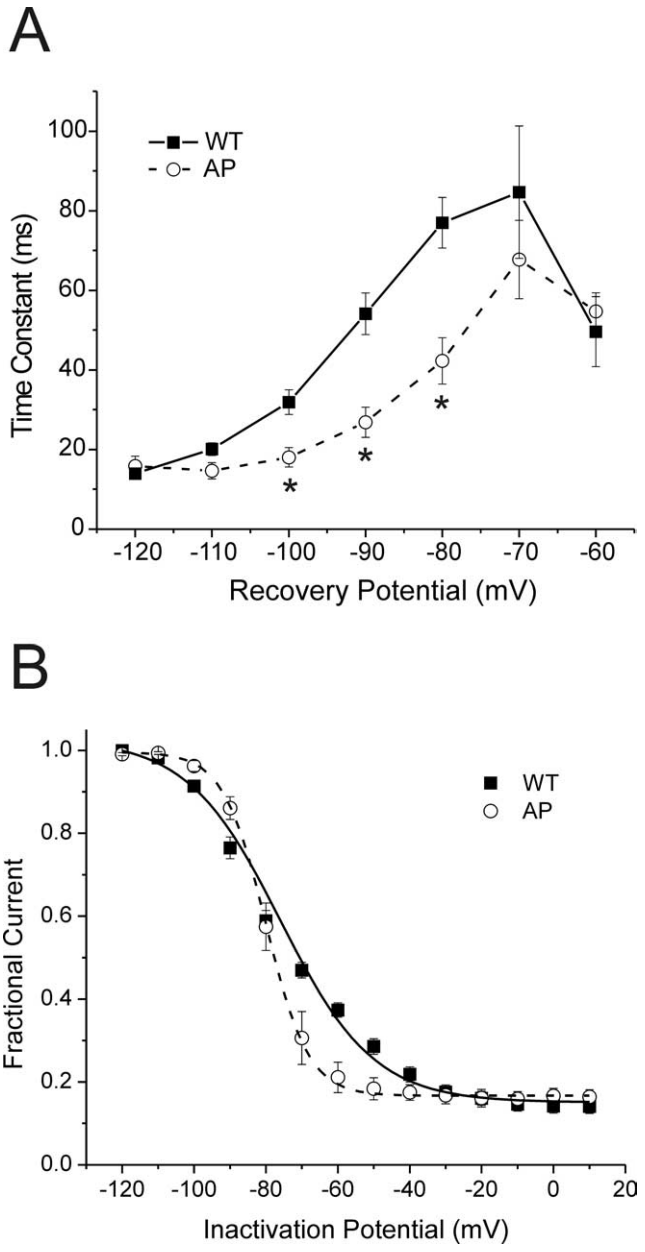

Figure 5. The A863P mutation alters recovery from fast inactivation and the voltage dependence of slow inactivation. ***A***, Voltage dependence of recovery from steady-state fast inactivation. From a holding potential of −100 mV, fast inactivation was initiated by a step to 0 mV for 20 ms, followed by a hyperpolarizing step to a recovery potential that varied in time (2–300 ms) and amplitude (−120 to −60 mV). The recovery period was followed by a second depolarizing test pulse to 0 mV. For each recovery potential, the peak inward current in response to the test pulse was normalized by the amplitude of the response to the inactivation step and plotted as a function of recovery period duration. These points were fit with a single exponential and plotted as a function of recovery membrane potential for cells expressing WT channels (■; $n = 17$) and A863P (AP) channels (○; $n = 10$). *$p < 0.05$. ***B***, Voltage dependence of steady-state slow inactivation for cells expressing WT (■; $n = 16$) and A863P (○; $n = 10$) sodium channels. Channels were first inactivated by a 30 s step to a membrane potential that varied from −120 mV to 10 mV, followed by a brief hyperpolarization (−120 mV for 100 ms) to remove fast inactivation and a depolarizing test pulse to 0 mV. Peak inward currents were normalized, plotted as a function of inactivation potential, and fit with a Boltzmann equation (solid line for WT; dotted line for A863P). Error bars represent SE.

Current-clamp electrophysiology

In one set of experiments, we investigated the effect of expressing WT channels on the firing properties of electroporated DRG neurons. Current-clamp recording conditions were used to deter-

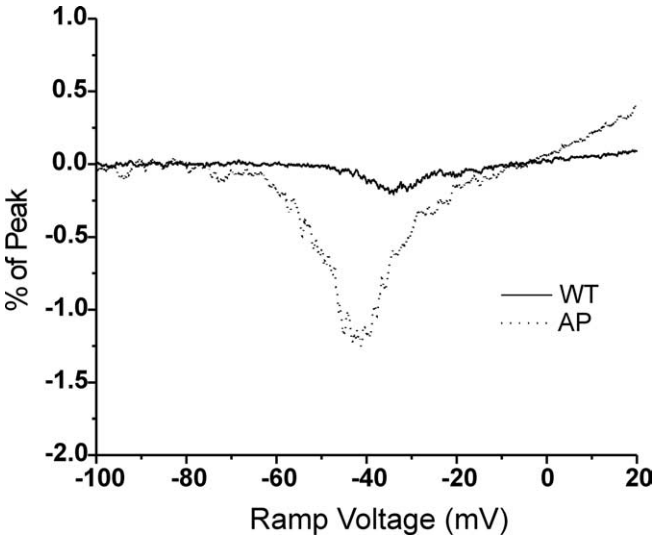

Figure 6. A863P mutation increases the size of currents elicited by slow ramp depolarizations. To elicit ramp currents, HEK293 cells held at −100 mV were stimulated with a depolarizing voltage ramp that increased to 20 mV over 600 ms (0.2 mV/ms). The current recorded during the ramp was expressed as a percentage of the peak inward current obtained during the initial activation protocol performed 3 min after breaking into the cell. Data from a cell expressing WT channels and a cell expressing A863P (AP) channels are represented by a solid line and dotted line, respectively.

mine input resistance, RMP, action potential threshold, and firing frequency in small (20–25 μm) DRG neurons transfected with GFP alone or GFP plus the WT $Na_v1.7$ DNA. As shown in Table 1, input resistance, spike amplitude, RMP, and the number of cells exhibiting repetitive firing were not significantly different for the two groups of cells. The frequency of repetitive firing for 1 s current steps of 50–1000 pA also did not differ between the two groups. Action potential threshold was slightly lower for cells expressing the WT channel (244 ± 28 pA; $n = 25$) than for cells with GFP alone (265 ± 42 pA; $n = 24$), but the difference was not significant. Because we have demonstrated that the same WT construct produced functional sodium channels in HEK293 cells (this study) and in gene gun-transfected DRG neurons (Herzog et al., 2003), these results suggest that additional WT $Na_v1.7$ sodium channels do not alter firing properties of electroporated small DRG neurons.

To assess the effect of the A863P mutation on excitability, current-clamp recordings were obtained from DRG neurons transfected with GFP and either the $Na_v1.7$ WT or the A863P construct. For the two groups of cells, there were no significant differences in input resistance or spike amplitude (Table 2). There was a small but significant difference in RMP. Cells expressing the A863P channels (−50.4 ± 1.4 mV; $n = 31$) were depolarized by 6.5 mV compared with cells expressing the WT channels (−56.9 ± 1.4 mV; $n = 32$; $t = 3.34$; $p < 0.01$). The two groups of cells also differed with regard to action potential threshold. As illustrated in Figure 7*A*, cells expressing WT channels responded to subthreshold current injections (100–300 pA) with graded membrane potential depolarizations. At threshold (310 pA for the cell in Fig. 7*A*), current injection produced an overshooting action potential, and further increases in injected current amplitude consistently resulted in one or more similar spikes. For WT channels, the threshold for action potential firing was 248 ± 32 pA ($n = 32$). Cells expressing the A863P mutation responded to current injections in a similar manner (Fig. 7*B*), but the threshold for action potential generation was significantly lower (157 ± 25 pA; $n = 31$; $p < 0.05$).

To examine the possibility that the depolarization of RMP produced by the A863P mutation was responsible for the decrease in threshold, we made additional current-clamp recordings in DRG neurons transfected with WT channels and measured the effect on threshold of depolarizing RMP by an amount similar to that produced by the mutant channel (6.5 mV). We found that in DRG neurons expressing the WT channel, depolarization (6.2 ± 0.6 mV) decreased threshold from 265 ± 54 pA before depolarization to 220 ± 42 pA after depolarization ($n = 13$; $p < 0.01$). We also performed the converse experiment, measuring the effect on threshold of hyperpolarization (6.7 ± 0.8 mV) in DRG neurons transfected with mutant A863P channels, and observed an increase in threshold from 178 ± 45 pA before hyperpolarization to 206 ± 46 pA after hyperpolarization ($n = 11$; $p < 0.01$). These experiments show that the change in RMP produced by the mutant channels contributes to the change in action potential threshold. The decrease in threshold for WT channels and A863P channels (36%) was larger than the decreases produced by depolarization of WT channels (16%) or hyperpolarization of A863P channels (21%), suggesting an additional effect on threshold of the A863P mutation.

In response to prolonged (1 s), suprathreshold current injections, ~50% of small DRG neurons generate multiple action potentials (Renganathan et al., 2001). In this study, a similar percentage of cells fired repetitively (Table 2) whether expressing WT $Na_v1.7$ channels (41%) or the A863P mutant channels (52%). However, there were significant differences in the frequency of firing across a broad range of current injections (50–500 pA). As shown in Figure 8*A*, cells expressing WT channels were more likely to generate only one or two additional spikes when stimulated with current injections that were two and three times the action potential threshold. In contrast, cells expressing the A863P mutation tended to fire with higher frequency bursting in response to similar stimuli (Fig. 8*B*). These results are summarized in Figure 8*C*. The increased firing frequency observed in cells expressing A863P mutant channels ($n = 31$), compared with cells expressing WT channels ($n = 32$), was significant for current injection amplitudes from 50 to 400 pA.

Discussion

In this study, we investigated the functional effect of A863P substitution in $Na_v1.7$ associated with IEM, a painful neuropathic disorder. Together with A863P, eight mutations in $Na_v1.7$ have been identified from 10 families with IEM (Yang et al., 2004; Dib-Hajj et al., 2005; Drenth et al., 2005; Michiels et al., 2005; Han et al., 2006). The $Na_v1.7$ mutations studied thus far by current clamp render small DRG neurons (a majority of which are nociceptive) hyperexcitable, a change that contributes to neuropathic pain (Dib-Hajj et al., 2005; Rush et al., 2006). These findings support the hypothesis that IEM is caused by mutations in $Na_v1.7$ channels, which are preferentially expressed in DRG and sympathetic neurons.

S5 segments contribute to sodium channel pore structure, whereas evidence suggests that S4–S5 intracellular linkers contribute to the receptor for the fast-inactivation tripeptide IFM (Smith and Goldin, 1997; McPhee et al., 1998). The $Na_v1.7$ DII/S4–S5 linker (Yang et al., 2004; Drenth et al., 2005; Han et al., 2006) and DII/S5 (this study) house ~50% of the mutations that have been associated with IEM. Mutations at these sites are likely to be functionally important, either because they interfere with direct binding to other channel sequences or because they have an allosteric effect, which could influence structures at a distance from the mutant site in the primary sequence. A863P substitution is expected to cause a bend in the α-helical structure of S5

Table 1. Current-clamp properties of DRG cells transfected with GFP alone or with GFP plus WT $Na_v1.7$

	N	R_{input} (MΩ)	RMP (mV)	Threshold (pA)	Spike amplitude (mV)	Repetitive firing
GFP	24	675 ± 69	−55.2 ± 1.3	265 ± 42	103 ± 4	9 of 24
WT	25	666 ± 70	−55.8 ± 0.9	244 ± 28	104 ± 3	9 of 25

Table 2. Current-clamp properties of DRG cells transfected with the WT $Na_v1.7$ or the A863P mutation

	N	R_{input} (MΩ)	RMP (mV)	Threshold (pA)	Spike amplitude (mV)	Repetitive firing
WT	32	589 ± 52	−56.9 ± 1.4	248 ± 32	111 ± 2	13 of 32
A863P	31	728 ± 68	−50.4 ± 1.4*	157 ± 25**	109 ± 2	16 of 31

*$p < 0.01$ compared to WT; **$p < 0.05$ compared to WT.

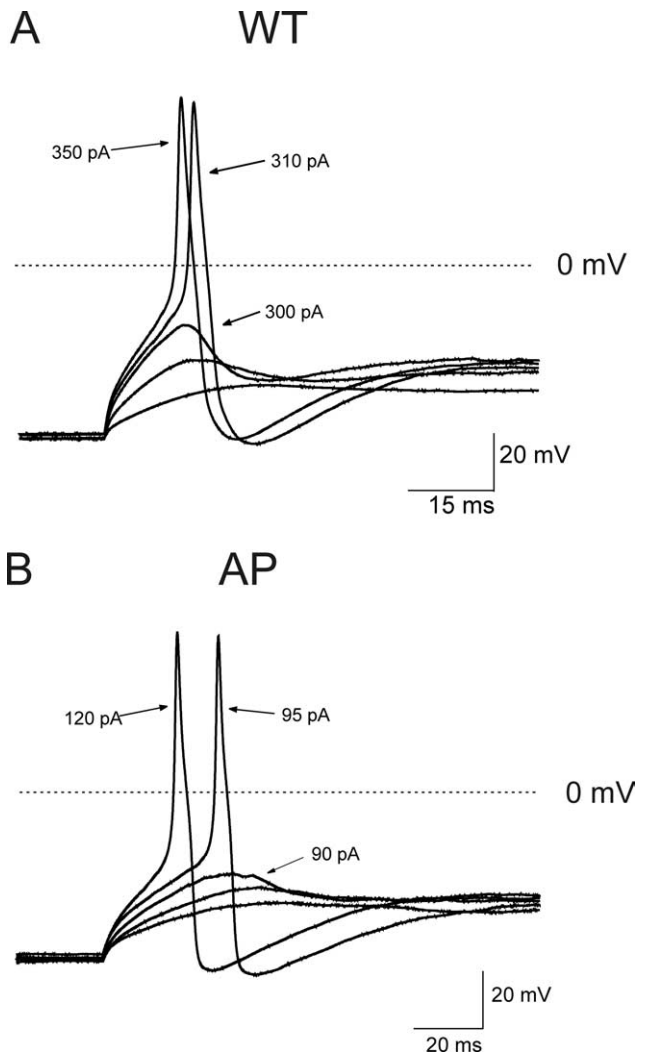

Figure 7. A863P mutation decreases action potential threshold in small, current-clamped DRG neurons. ***A***, Responses of a current-clamped DRG neuron transfected with WT $Na_v1.7$ DNA to a series of subthreshold and suprathreshold depolarizing current steps. Starting at a subthreshold stimulus intensity, the current amplitude was increased in 5 pA increments to an intensity well beyond threshold. The RMP for this cell was −55 mV, and the threshold was 310 pA. ***B***, The same threshold protocol applied to a DRG neuron transfected with the A863P (AP) mutant DNA. The RMP for this cell was −45 mV, and the threshold was 95 pA. Arrows with numbers indicate the current step amplitude used to elicit the labeled response.

and disrupt the normal intrahelical interactions or interhelical interactions with other channel segments, leading to altered conformations with functional consequences. Indeed, substitution of a glycine residue by proline (G219P) in S6 of bacterial voltage-gated sodium channels produces a 50 mV depolarizing shift in activation, a 2000-fold slowing of deactivation, and a 1200-fold reduction in the rate of voltage-dependent inactivation (Zhao et al., 2004). A863P showed similar but more modest changes in these gating properties. The effect of G219P on the gating properties of the bacterial channel was explained by proposing a stronger bending of S6 at the hinge residue, G219 (Zhao et al., 2004). By analogy, A863P might be expected to introduce a bend in the α-helical structure of S5, biasing the open state of the channel.

Different sodium channel isoforms may tolerate mutations in S5 to different degrees. The $Na_v1.4$ mutants T704M in DII/S5 and I1495F in DIV/S5, which have been linked to hyperkalemic periodic paralysis (Cannon and Strittmatter, 1993; Cummins et al., 1993; Bendahhou et al., 1999), shift voltage dependence of activation in a hyperpolarizing direction, whereas L266V in DI/S5 produces a depolarizing shift in steady-state inactivation but no effect on activation (Wu et al., 2001). Mutation F1344S in DIII/S5 in $Na_v1.5$ causes Brugada syndrome and shifts activation in a depolarizing direction (Keller et al., 2006). Several mutations in S5 segments of domains II, III, and IV of $Na_v1.1$ render the channel nonfunctional (Lossin et al., 2003; Fukuma et al., 2004; Rhodes et al., 2004). Thus, mutations in S5 of different sodium channel isoforms have diverse effects, and their impact on pathophysiology has to be empirically determined.

Our findings on the biophysical properties of A863P support a direct role for this mutation in the pathophysiology of IEM. Activation is shifted so that the voltage threshold for opening is more hyperpolarized for mutant channels, whereas steady-state inactivation is shifted in a depolarizing direction, increasing the number of channels that are available to open at more depolarized potentials compared with WT channels. Closed-state inactivation is also shifted in the depolarizing direction, so that more $Na_v1.7$ channels are available to open near resting potential. The decreased rate of deactivation means that channels stay open longer after stimulus offset, which further enhances excitability. One consequence of these biophysical changes is that mutant channels produce larger responses to slow depolarizations, which may contribute to a reduction in action potential threshold.

In current-clamp recordings, the A863P mutation clearly produced hyperexcitability, manifested by lower action potential threshold and increased frequency of firing. These changes presumably are attributable to changes in biophysical properties of $Na_v1.7$ sodium channels, although not all of the biophysical changes produced by the A863P mutation are predicted to contribute to hyperexcitability in small DRG neurons. Closed-state inactivation develops more quickly at hyperpolarized inactivation potentials (−90 to −80 mV), and the slope of the voltage dependence of slow inactivation increases in cells expressing A863P (Fig. 5*B*). Thus, at membrane potentials more positive than the midpoint of inactivation (approximately −80 mV for both WT and A863P channels), a larger fraction of channels are inactivated (e.g., ~20% more at −60 mV), leading to a decrease in excitability. However, based on the present results and data from previously characterized mutations (Rush et al., 2006), we conclude that $Na_v1.7$ mutations can produce a depolarization in RMP and that a depolarization of RMP leads to a reduction in the threshold of small DRG neurons.

We have provided evidence that mutant $Na_v1.7$ channels can depolarize the RMP of DRG neurons because of an increase in a

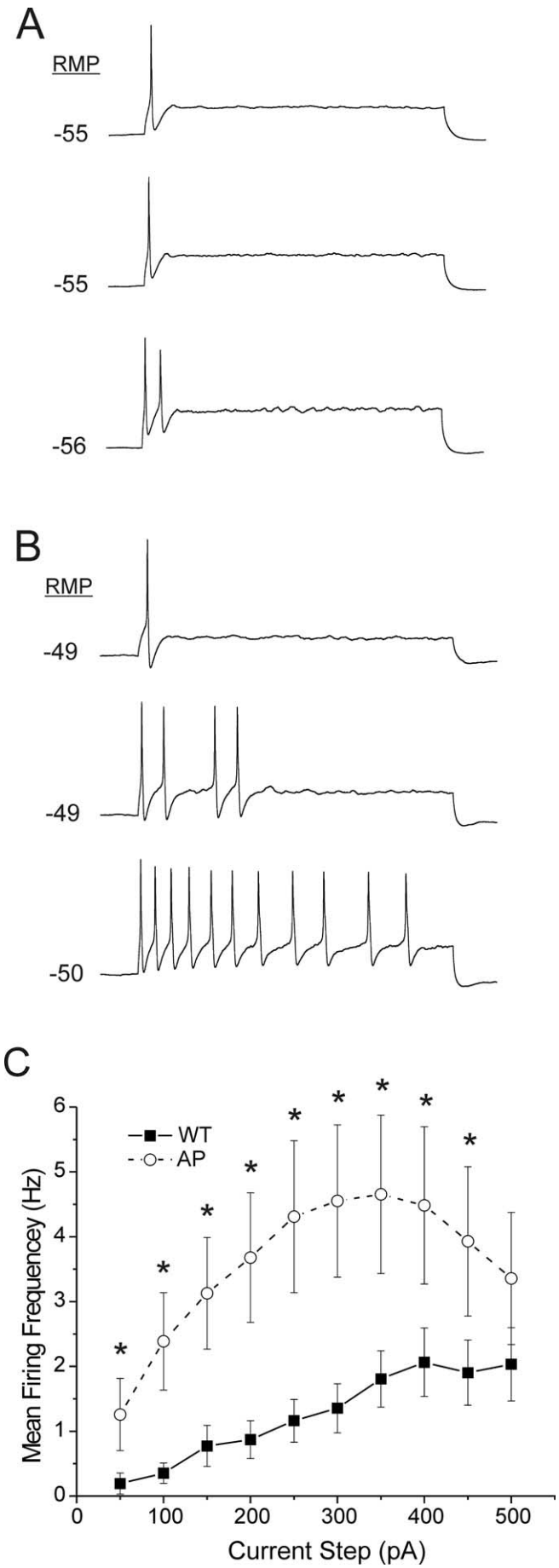

window current produced by overlapping activation and inactivation processes. Based on currents recorded in HEK293 cells (this study) and isolation of TTX-r currents in small DRG neurons from $Na_v1.8-/-$ animals (Herzog et al., 2003) that were gene-gun transfected with the same WT $Na_v1.7$ construct used in this study, it is reasonable to assume expression of the WT construct in our current-clamp experiments. Our calculations also predict a much smaller window current and a negligible contribution of WT channels to RMP, a prediction supported by the absence of a significant difference in RMP for cells transfected with GFP alone compared with GFP plus WT construct. Control experiments also suggest that adding WT channels to DRG neurons does not alter threshold. It remains to be determined whether depolarization of RMP accounts for the entire change in threshold produced by the A863P mutation. Our results indicate that depolarization imposed by injection of current accounts for about one-half of the decrease in threshold that accompanies a similar depolarization produced by the A863P mutation and suggest that additional factors may contribute to the decrease in threshold. This possibility is supported by data from the $Na_v1.7$ F1449V mutation, which fails to significantly depolarize the RMP of small DRG neurons, yet produces a significant decrease in action potential threshold (Dib-Hajj et al., 2005).

One additional factor that may play a role in decreasing threshold is the increase in the response of mutant channels to slow depolarizations. In small DRG neurons, ramp currents have been attributed to slow closed-state inactivation of $Na_v1.7$ channels (Cummins et al., 1998), which leaves more channels in an available state in response to slow depolarizing stimuli. Because they can be evoked close to RMP, ramp currents may serve to amplify inputs that ordinarily would not lead to spike initiation. The observation that increases in ramp current amplitude are accompanied by decreases in spike threshold for $Na_v1.7$ mutants L858H (Rush et al., 2006) and A863P (this study) suggests an association between these two phenomena. In contrast, data from F1449V demonstrate that changes in threshold are not necessarily accompanied by changes in ramp current amplitude (Dib-Hajj et al., 2005). The biophysical changes produced by the F1449V mutant mirror changes produced by the A863P mutant in all but two respects: the F1449V mutant does not decrease the rate of deactivation and does not enhance the ramp current. This observation leads to two interesting conclusions: (1) ramp currents are influenced strongly by deactivation rate, because the only two differences between F1449V and A863P are deactivation and ramp current, and (2) other factors in addition to RMP depolarization and ramp current can influence spike threshold, which was decreased by the F1449V mutation without changes in RMP or ramp current.

If depolarization of RMP inactivates most sodium channels, thereby reducing excitability, as observed in sympathetic ganglion neurons transfected with the L858H mutation (Rush et al., 2006), why do DRG neurons become hyperexcitable? DRG neurons are unique in expressing $Na_v1.8$ channels (Akopian et al.,

←

Figure 8. Increased frequency of firing in current-clamped DRG neurons expressing A863P mutant channels. ***A***, Response of a cell expressing WT channels to 1 s depolarizing current steps that are one, two, and three (top, middle, and bottom traces, respectively) times the current threshold for action potential generation. ***B***, The same stimulus protocol for a cell expressing A863P mutant channels. ***C***, Summary of firing frequency data. The total number of action potentials (defined as spikes in membrane potential >0 mV) elicited by the indicated depolarizing current step for cells expressing WT (■; $n = 32$) and A863P (AP; ○; $n = 31$) channels. RMPs are expressed in millivolts. Error bars represent SE. *$p < 0.05$.

1996; Black et al., 1996; Sangameswaran et al., 1996), as well as $Na_v1.7$. $Na_v1.8$ differs from other voltage-gated sodium channels in that its voltage dependence of inactivation is shifted in a depolarizing direction, with a $V_{1/2}$ of about −30 mV (Akopian et al., 1996; Sangameswaran et al., 1996; Catterall et al., 2005). Thus, $Na_v1.8$ channels are not inactivated in neurons expressing the A863P mutation, although the mutation depolarizes the cells. Because $Na_v1.8$ channels produce up to 80% of the current underlying the action potential upstroke in cells in which they are present (Renganathan et al., 2001; Blair and Bean, 2002), the membrane potential associated with spike initiation is unlikely to be changed by transfection with WT or A863P $Na_v1.7$. A physiological link between $Na_v1.7$ and $Na_v1.8$ is predicted to contribute to DRG neuron excitability, with mutant $Na_v1.7$ boosting otherwise subthreshold stimuli and $Na_v1.8$ contributing to the depolarizing phase of the action potential. The predicted physiological coupling of $Na_v1.7$ and $Na_v1.8$ has recently been shown to account, at least in part, for the differential response of DRG and sympathetic neurons to the presence of mutant $Na_v1.7$ channels (Rush et al., 2006).

References

Akopian AN, Sivilotti L, Wood JN (1996) A tetrodotoxin-resistant voltage-gated sodium channel expressed by sensory neurons. Nature 379:257–262.

Bendahhou S, Cummins TR, Tawil R, Waxman SG, Ptacek LJ (1999) Activation and inactivation of the voltage-gated sodium channel: role of segment S5 revealed by a novel hyperkalaemic periodic paralysis mutation. J Neurosci 19:4762–4771.

Black JA, Dib-Hajj S, McNabola K, Jeste S, Rizzo MA, Kocsis JD, Waxman SG (1996) Spinal sensory neurons express multiple sodium channel alpha-subunit mRNAs. Brain Res Mol Brain Res 43:117–131.

Black JA, Liu S, Tanaka M, Cummins TR, Waxman SG (2004) Changes in the expression of tetrodotoxin-sensitive sodium channels within dorsal root ganglia neurons in inflammatory pain. Pain 108:237–247.

Blair NT, Bean BP (2002) Roles of tetrodotoxin (TTX)-sensitive Na^+ current, TTX-resistant Na^+ current, and Ca^{2+} current in the action potentials of nociceptive sensory neurons. J Neurosci 22:10277–10290.

Cannon SC, Strittmatter SM (1993) Functional expression of sodium channel mutations identified in families with periodic paralysis. Neuron 10:317–326.

Catterall WA, Goldin AL, Waxman SG (2005) International Union of Pharmacology. XLVII. Nomenclature and structure-function relationships of voltage-gated sodium channels. Pharmacol Rev 57:397–409.

Cummins TR, Zhou J, Sigworth FJ, Ukomadu C, Stephan M, Ptacek LJ, Agnew WS (1993) Functional consequences of a Na+ channel mutation causing hyperkalemic periodic paralysis. Neuron 10:667–678.

Cummins TR, Howe JR, Waxman SG (1998) Slow closed-state inactivation: a novel mechanism underlying ramp currents in cells expressing the hNE/PN1 sodium channel. J Neurosci 18:9607–9619.

Cummins TR, Dib-Hajj SD, Waxman SG (2004) Electrophysiological properties of mutant $Na_v1.7$ sodium channels in a painful inherited neuropathy. J Neurosci 24:8232–8236.

Dib-Hajj SD, Rush AM, Cummins TR, Hisama FM, Novella S, Tyrrell L, Marshall L, Waxman SG (2005) Gain-of-function mutation in Nav1.7 in familial erythromelalgia induces bursting of sensory neurons. Brain 128:1847–1854.

Drenth JP, te Morsche RH, Guillet G, Taieb A, Kirby RL, Jansen JB (2005) SCN9A mutations define primary erythermalgia as a neuropathic disorder of voltage gated sodium channels. J Invest Dermatol 124:1333–1338.

Finley WH, Lindsey Jr JR, Fine JD, Dixon GA, Burbank MK (1992) Autosomal dominant erythromelalgia. Am J Med Genet 42:310–315.

Fukuma G, Oguni H, Shirasaka Y, Watanabe K, Miyajima T, Yasumoto S, Ohfu M, Inoue T, Watanachai A, Kira R, Matsuo M, Muranaka H, Sofue F, Zhang B, Kaneko S, Mitsudome A, Hirose S (2004) Mutations of neuronal voltage-gated Na+ channel alpha 1 subunit gene SCN1A in core severe myoclonic epilepsy in infancy (SMEI) and in borderline SMEI (SMEB). Epilepsia 45:140–148.

Han C, Rush AM, Dib-Hajj SD, Li S, Xu Z, Wang Y, Tyrrell L, Wang X, Yang Y, Waxman SG (2006) Sporadic onset of erythermalgia: a gain-of-function mutation in Nav1.7. Ann Neurol 59:553–558.

Herzog RI, Cummins TR, Ghassemi F, Dib-Hajj SD, Waxman SG (2003) Distinct repriming and closed-state inactivation kinetics of Nav1.6 and Nav1.7 sodium channels in mouse spinal sensory neurons. J Physiol (Lond) 551:741–750.

Keller DI, Huang H, Zhao J, Frank R, Suarez V, Delacretaz E, Brink M, Osswald S, Schwick N, Chahine M (2006) A novel SCN5A mutation, F1344S, identified in a patient with Brugada syndrome and fever-induced ventricular fibrillation. Cardiovasc Res 70:521–529.

Klugbauer N, Lacinova L, Flockerzi V, Hofmann F (1995) Structure and functional expression of a new member of the tetrodotoxin-sensitive voltage-activated sodium channel family from human neuroendocrine cells. EMBO J 14:1084–1090.

Lossin C, Wang DW, Rhodes TH, Vanoye CG, George Jr AL (2002) Molecular basis of an inherited epilepsy. Neuron 34:877–884.

Lossin C, Rhodes TH, Desai RR, Vanoye CG, Wang D, Carniciu S, Devinsky O, George Jr AL (2003) Epilepsy-associated dysfunction in the voltage-gated neuronal sodium channel SCN1A. J Neurosci 23:11289–11295.

McPhee JC, Ragsdale DS, Scheuer T, Catterall WA (1998) A critical role for the S4–S5 intracellular loop in domain IV of the sodium channel alpha-subunit in fast inactivation. J Biol Chem 273:1121–1129.

Michiels JJ, te Morsche RH, Jansen JB, Drenth JP (2005) Autosomal dominant erythermalgia associated with a novel mutation in the voltage-gated sodium channel alpha subunit Nav1.7. Arch Neurol 62:1587–1590.

Nassar MA, Stirling LC, Forlani G, Baker MD, Matthews EA, Dickenson AH, Wood JN (2004) Nociceptor-specific gene deletion reveals a major role for Nav1.7 (PN1) in acute and inflammatory pain. Proc Natl Acad Sci USA 101:12706–12711.

Nathan A, Rose JB, Guite JW, Hehir D, Milovcich K (2005) Primary erythromelalgia in a child responding to intravenous lidocaine and oral mexiletine treatment. Pediatrics 115:e504–e507.

Renganathan M, Cummins TR, Waxman SG (2001) Contribution of Na(v)1.8 sodium channels to action potential electrogenesis in DRG neurons. J Neurophysiol 86:629–640.

Rhodes TH, Lossin C, Vanoye CG, Wang DW, George Jr AL (2004) Noninactivating voltage-gated sodium channels in severe myoclonic epilepsy of infancy. Proc Natl Acad Sci USA 101:11147–11152.

Rizzo MA, Kocsis JD, Waxman SG (1994) Slow sodium conductances of dorsal root ganglion neurons: intraneuronal homogeneity and interneuronal heterogeneity. J Neurophysiol 72:2796–2815.

Rush AM, Craner MJ, Kageyama T, Dib-Hajj SD, Waxman SG, Ranscht B (2005) Contactin regulates the current density and axonal expression of tetrodotoxin-resistant but not tetrodotoxin-sensitive sodium channels in DRG neurons. Eur J Neurosci 22:39–49.

Rush AM, Dib-Hajj SD, Liu S, Cummins TR, Black JA, Waxman SG (2006) A single sodium channel mutation produces hyper- or hypoexcitability in different types of neurons. Proc Natl Acad Sci USA 103:8245–8250.

Sangameswaran L, Delgado SG, Fish LM, Koch BD, Jakeman LB, Stewart GR, Sze P, Hunter JC, Eglen RM, Herman RC (1996) Structure and function of a novel voltage-gated, tetrodotoxin-resistant sodium channel specific to sensory neurons. J Biol Chem 271:5953–5956.

Sangameswaran L, Fish LM, Koch BD, Rabert DK, Delgado SG, Ilnicka M, Jakeman LB, Novakovic S, Wong K, Sze P, Tzoumaka E, Stewart GR, Herman RC, Chan H, Eglen RM, Hunter JC (1997) A novel tetrodotoxin-sensitive, voltage-gated sodium channel expressed in rat and human dorsal root ganglia. J Biol Chem 272:14805–14809.

Smith MR, Goldin AL (1997) Interaction between the sodium channel inactivation linker and domain III S4–S5. Biophys J 73:1885–1895.

Toledo-Aral JJ, Moss BL, He ZJ, Koszowski AG, Whisenand T, Levinson SR, Wolf JJ, Silos-Santiago I, Halegoua S, Mandel G (1997) Identification of PN1, a predominant voltage-dependent sodium channel expressed principally in peripheral neurons. Proc Natl Acad Sci USA 94:1527–1532.

van Genderen PJ, Michiels JJ, Drenth JP (1993) Hereditary erythermalgia and acquired erythromelalgia. Am J Med Genet 45:530–532.

Wu FF, Takahashi MP, Pegoraro E, Angelini C, Colleselli P, Cannon SC, Hoffman EP (2001) A new mutation in a family with cold-aggravated myotonia disrupts Na(+) channel inactivation. Neurology 56:878–884.

Yang Y, Wang Y, Li S, Xu Z, Li H, Ma L, Fan J, Bu D, Liu B, Fan Z, Wu G, Jin J, Ding B, Zhu X, Shen Y (2004) Mutations in SCN9A, encoding a sodium channel alpha subunit, in patients with primary erythermalgia. J Med Genet 41:171–174.

Zhao Y, Scheuer T, Catterall WA (2004) Reversed voltage-dependent gating of a bacterial sodium channel with proline substitutions in the S6 transmembrane segment. Proc Natl Acad Sci USA 101:17873–17878.